ELSEVIER

Surface Science 356 (1996) 144–160

surface science

Reconstruction kinetics of a stepped metallic surface: step doubling and singling of Ni(977) induced by low oxygen coverages

L. Niu [a,b,1], D.D. Koleske [a,c,2], D.J. Gaspar [a,c], S.F. King [a,c,3], S.J. Sibener [a,c,*]

[a] *The James Franck Institute, The University of Chicago, 5640 S. Ellis Ave., Chicago, IL 60637, USA*
[b] *Department of Physics, The University of Chicago, Chicago, IL, USA*
[c] *Department of Chemistry, The University of Chicago, Chicago, IL, USA*

Received 14 August 1995; accepted for publication 28 December 1995

Abstract

Helium atom diffraction has been used to study the reconstruction kinetics of a stepped metallic surface, Ni(977), which sequentially undergoes step-doubling and -singling upon dosing with low coverages of oxygen. Over the temperature range 390–470 K it was found that less than 2% of a monolayer of oxygen was sufficient to transform the initially prepared single-stepped surface to a new steady state having a double-stepped structure. The thermal range over which the doubled phase exists extends to higher temperatures when more oxygen is present. At low oxygen exposures this doubled interface reverts to the single-stepped surface above 470 K. Singling can also be driven by more extensive levels of oxygen adsorption. The kinetics of the step-doubling transformation which occurs below 470 K was determined to be second order with respect to single-step density while, for temperatures above 470 K, step-singling followed first-order kinetics with respect to the double-step density. Oxygen atoms adsorbed at step edges play a crucial role in these transformations. Arrhenius analysis is used to extract energetics for the step-doubling and -singling reconstructions. These results delineate the sequence of mechanistic stages which occur during the initial stages of oxidation of a stepped metallic interface which precede the onset of bulk oxidation, findings which are important for developing an improved understanding of metallic oxidation and corrosion.

Keywords: Atom–solid scattering diffraction – elastic; Corrosion Models of surface kinetics; Nickel; Oxidation; Stepped single crystal surfaces; Surface relaxation and reconstruction; Surface structure, morphology, roughness, and topography;

1. Introduction

Stepped (vicinal) single crystal surfaces are very informative model systems for probing the chemical, physical, and metallurgical properties of imperfect surfaces. Careful preparation of such surfaces allows one to produce samples having known crystallographic orientation and hence controlled numbers and types of interfacial defects. In this paper we will focus on the structural changes which one such vicinal surface, Ni(977), undergoes upon the adsorption of small quantities of oxygen, a reaction regime which we have found to exhibit extensive structural transformations which precede the onset of bulk metallic oxidation. Knowledge of such adsorbate-induced behavior contributes to our fundamental understanding of interface ener-

[1] Current Address: AT&T Bell Labs, Bldg. 510E, Upton, NY 11973, USA.
[2] Current Address: Naval Research Laboratory, Washington, DC 20375, USA.
[3] Current Address: US Environmental Protection Agency, Chicago, IL, USA.
* Corresponding author. Fax: +1 312 702 5863.

PII S0039-6028(96)00032-5

getics and stability, central issues in our quest for a refined understanding of metallic oxidation and corrosion, surface passivation, chemical catalysis, and crystal growth. Examples include the crucial role that defect sites such as steps and kinks play in altering the rates and pathways of surface chemical reactions, including the onset of metallic corrosion.

The morphological transitions induced by the presence of adsorbates on stepped surfaces permit us to examine how steps modify the behavior exhibited by smooth, i.e., nearly perfect, crystallographic planes [1]. It is becoming apparent that many vicinal surfaces undergo extensive structural transitions/reconstructions due to the presence of adsorbates such as oxygen and sulfur [1–14]. Perhaps the earliest study of oxygen induced step-doubling was by Lang et al. [2] for Pt(554). In another early study Blakely and Somorjai [3] examined morphological transitions on vicinal Pt surfaces when the surface was either clean or covered with monolayers of chemisorbed oxygen or carbon. Thapliyal et al. [4,5] observed morphological transitions on clean or carbon-covered vicinal Ni(111) surfaces; recent work on Ni(111)5°[112] by Chang and Blakely [6] find similar behavior. Similar effects have also been seen for Rh(775) [7] and Ni(771) [8,9]. A connected literature dealing with doubling and faceting also exists for clean semiconductor interfaces [15–17], whose reconstruction behavior can differ from metals due to strong directional bonding and the presence of robust superlattices. Of particular relevance to the work reported herein was the kinetic study performed by Comsa and co-workers on the oxygen-induced step-doubling of Pt(997) examined in the limit of relatively high amounts of adsorbed oxygen [10]. These helium diffraction measurements were analyzed assuming that the kinetics of this transition were first order with respect to the single step density. They were also able to form an oxygen-free double-stepped surface by using hydrogen to react away the oxygen, and were therefore able to study the kinetics of step-singling for the clean double-stepped surface, again assuming first-order kinetics. Hoogers and King [11] recently observed step-doubling and step-singling (i.e., undoubling) on Rh(332) surfaces with 0.1 and 0.6 ML oxygen, respectively. Their modelling of the experimental data showed that the kinetics for doubling and singling could be fit by second-order kinetics with respect to single and double steps, respectively. Taken together, these findings suggest that the kinetics of such reconstructive transitions may depend not only on the metal and crystallographic plane being studied, but also on the amount of oxygen present and the temperature regime being studied – findings which suggest that surface morphology plays a crucial role in the atomic level dynamics of such transformations.

Other results from our laboratory [14] have demonstrated the existence of a remarkably rich series of oxygen-driven reconstructive transformations for Ni(977), primarily focussing on relatively high levels of oxygen exposure. The actual details of these large-scale reconstructions, such as phase stability regimes, strongly depend on oxygen coverage, sub-surface oxygen content (and, hence, sample history) and surface temperature. For example, we have previously shown in the limit of relatively high oxygen coverages that the initial step-doubling transformation can be reversed by the subsequent addition of more oxygen to the system, i.e., step-singling occurs upon continuing oxygen exposure, as shown in Fig. 1. This is a thermodynamically stable regime which we now know precedes the onset of bulk oxidation at moderate temperatures. The data shown in this figure are for a helium diffraction experiment conducted with the scattering plane aligned perpendicular to, i.e., across, the step direction. It shows about one hour of continuous isothermal oxidation data (surface temperature, T_s, held at 500 K while exposing the surface to a constant O_2 pressure of 4×10^{-10} Torr). At the beginning of this run, helium diffraction yields two distinct diffraction peaks, characteristic for out-of-phase (anti-Bragg) scattering from the clean single-stepped surface. As oxidation continues, one can clearly see the appearance and growth of a third diffraction peak centered between the two initially present peaks. This is the diffraction signature for the double-stepped surface under in-phase (Bragg) scattering conditions (see Section 2 for technical details about the choice and purpose of using in- and out-of-phase

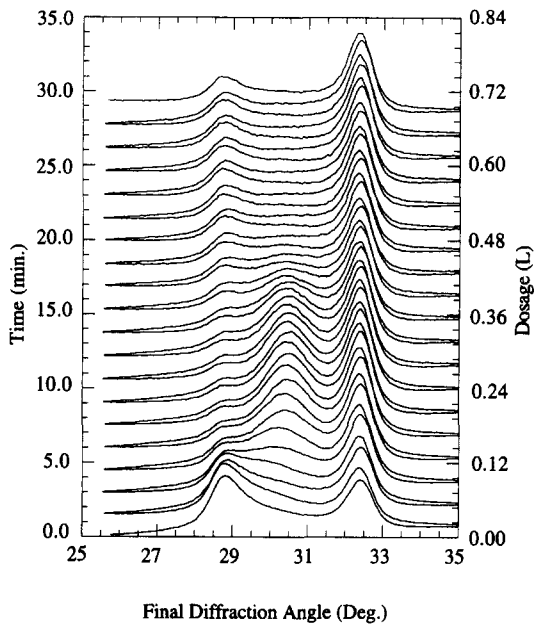

Fig. 1. Structural evolution of Ni(977) surface while dosing with 4×10^{-10} Torr of oxygen at a crystal temperature of 500 K. There are 40 sequential helium diffraction runs, with each run taking 40 s. Scattering is across the steps in the "downstairs" direction ($\theta_i=30.4°$, $E_i=20.7$ meV) with θ_i measured from the terrace normal.

scattering conditions). The y-axis in this plot is linearly proportional to time, and hence oxygen exposure. This figure clearly shows the evolution from the initially prepared clean and single-stepped surface to the double-stepped surface at low oxygen coverages and ultimately its return upon further oxygen exposure to a single-stepped structure.

In this paper we deal with the temperature and oxygen coverage dependent *kinetics* for step-doubling and subsequent singling transformations on Ni(977) induced by *relatively low coverages of oxygen*. We will show that this low coverage regime is a particularly informative one for exploring the nature of these transformations. Novel scattering methodologies based on constructive and destructive scattering interferences between adjacent terraces provide real-time (and quite sensitive) quantification of single- and double-step populations. These measurements complement our earlier structural work which examined oxidation at higher exposures of oxygen [14], including more extensive levels of bulk oxidation, as well as more recent work from our group on the oxidation kinetics of Ni(111) [18–20]. They are also a part of our larger thrust, which is to understand how surface forces influence, and correlate with, surface structure and chemical reactivity. Work from our group along these lines includes surface phonon measurements on clean [21] and oxygen-covered [22] Ni(111), which taken together show how oxygen adsorption can modify the surface force field on a smooth metallic interface. More recent work has moved this discussion to include vicinal (imperfect) surfaces, where surface phonon spectroscopy measurements of Ni(977) [23,24] have revealed the presence of step-induced phonon modes (as well as systematic changes in the terrace forces as compared to the (111) surface). Such modes hold the key to elucidating the binding forces present in the vicinity of low-bonding coordination sites – information central to the kinetic issues addressed in this paper.

2. Experimental

2.1. Instrumentation

Helium atom diffraction was used to monitor the structural reconstruction of the Ni(977) surface. Low energy neutral helium atom scattering is a nearly ideal probe for this system due to its exclusive surface sensitivity and high sensitivity to steps. Our helium-scattering instrument has been previously described in detail [24,25]. It is shown schematically in Fig. 2a, and can be viewed as consisting of three parts: beamline, scattering chamber, and rotating quadrupole based detector.

The supersonic atom beam source (UHP grade 99.999% helium) produces a nearly monochromatic incident flux of helium atoms (e.g., for $T_{nozzle}=112$ K: $\Delta\lambda/\lambda=0.66\%$) and utilizes a two-stage closed-cycle helium refrigeration system in order to operate at temperatures between ca. 40 and 300 K. Different incident wave vectors are generated by temperature tuning the nozzle tip to the desired setting. In most of this study, the kinetic energy of the helium beams was 22.0 meV and the incident angle θ_i was 33.4°. The beamline has three differential pumping regions: the first contains the

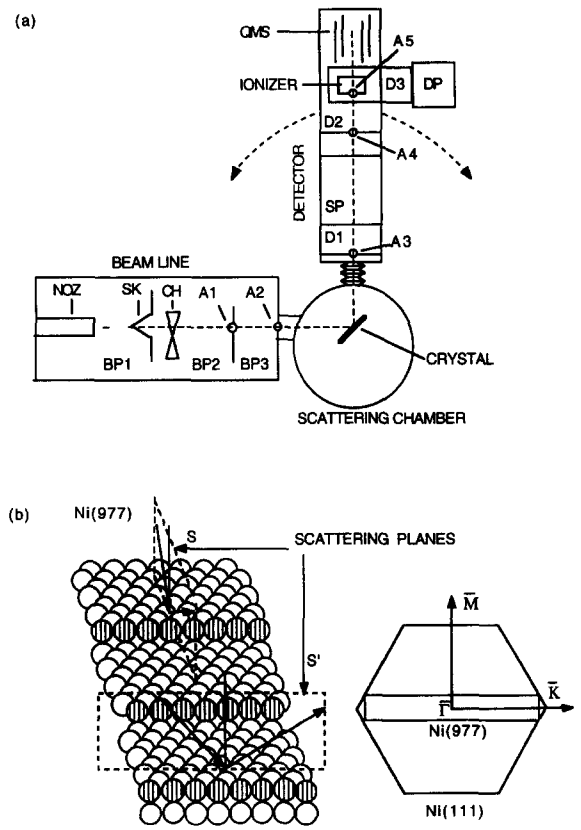

Fig. 2. Schematic view of our helium scattering machine is shown in (a). It consists three parts: beam line, scattering chamber and detector. Our sample Ni(977) is schematically illustrated in (b) where the two scattering planes are also designated.

nozzle-skimmer beam generation region, the next a dynamically balanced chopper disk (which contains multiple time-of-flight, diffraction, and cross-correlation modulation patterns), and the third acts as a buffer pumping chamber before the beam enters the scattering chamber. The scattering chamber is pumped by ion, Ti sublimation, and cryogenically baffled diffusion pumps. Added pumping speed comes from a two-stage closed-cycle helium refrigerator which we use for cooling the target assembly. Base pressures of ca. 7×10^{-11} Torr are routinely achieved with the helium beam off. The background pressure in the scattering chamber was 3.5×10^{-9} Torr during diffraction with 50% beam modulation. The Ni sample was mounted on a manipulator which allows for adjustment of the crucial degrees of freedom: sample XYZ translation, as well as tilt, azimuth, and polar angles. The manipulator rides on a large triple-differentially sealed rotary platform (using spring-loaded Teflon gaskets), and is mounted 5.08 cm from the center of flange rotation. This allows the sample to be rotated into a variety of positions in the scattering chamber such as the scattering center of the instrument, sputtering, LEED, Auger, etc. Finally, the detector consists of three differentially pumped regions which rotate, under computer control, by $\pm 20°$ around the scattering center. The actual detector consists of an electron bombardment ionizer/quadrupole mass spectrometer (the ionizer is separately nested in a turbomolecular-pumped region which is in turn backed by a diffusion pump to achieve high helium compression before evacuation by a mechanical pump). The entire detector assembly is mounted on an optical rail support system which permits changes in the flight-path between the crystal and the ionizer. In these studies we used the highest resolution "long flight-path" setting: chopper-to-crystal distance 55.1 cm and crystal-to-ionizer distance 101.5 cm. The composite energy and angular resolution parameters for the instrument as configured for these experiments were 0.46 meV and 0.36° (corresponding to a wavevector resolution of 0.038 $Å^{-1}$).

2.2. Sample preparation and oxygen/nickel metallurgy

The surface we studied was Ni(977), provided by Princeton Scientific Corp. It was prepared by cutting a Ni single crystal 7.02° away from the (111) plane along the $(2\bar{1}\bar{1})$ direction. The crystal orientation was verified to be within 0.5° of the ideal (977) direction with Laue X-ray back-reflection. The surface can also be labeled as Ni[8(111)×(100)] in microfacet notation [26], which indicates that the surface consists of (111) terraces that are 8 atomic rows wide and (ideally) straight (100) steps that are one atom high (Fig. 2b). The double-stepped surface, Ni[15(111)×2(100)], has two atom high (100) steps and 15 atom wide (111) terraces. The crystal was cleaned by Ar^+ sputtering during repetitive temperature cycles (between 500 and 1100 K) and

then annealed at 1100 K. Surface order was checked by LEED and He diffraction, and surface cleanliness by Auger spectroscopy. Oxygen was introduced to the sample chamber through a Varian leak valve with the exposure time lasting no more than 1 min at pressures typically in the range 4×10^{-10} through 5×10^{-9} Torr; unless otherwise noted, the sample was dosed at the temperature for a given kinetic measurement. This procedure allowed precise control of adsorbate exposure. Since the real-time kinetic runs took on the order of 10^3 s, the initial 1 min dosing transient is inconsequential. The oxygen coverages in this paper were estimated using the sticking coefficient data of Winkler et al. [27], who have reported that the sticking coefficient for O_2 on Ni(977) is 0.55 at zero coverage, decreasing to 0.35 at 0.1 ML coverage. (However, note that these sticking coefficients may be systematically too low, as discussed by Brundle and Broughton in their extensive review on this subject. [28] The same slowly decreasing trend in sticking coefficient as a function of oxygen exposure is suggested, but with a starting value closer to unity.) Throughout this paper we take 1 ML coverage to equal the Ni atom density of the (111) surface, 1.86×10^{15} atoms/cm^2.

Observations (such as changes in doubling behavior) indicate that the nickel sample is modified by repeated exposures to high levels of oxygen, especially at elevated temperatures. This behavior has also been noted by other groups working on Ni [28–30]. This induced us to conduct this low oxygen coverage study on a new sample before repeating and extending some of our older measurements involving more extensive oxygen exposures and deeper levels of bulk oxidation. (Only after completing this study did we intentionally expose the new sample to higher levels of oxygen; LEED studies reproduced the doubling/singling behavior exhibited by the original crystal [14] (Fig. 1).) Nevertheless, complications due to oxygen absorption into the near surface region (selvedge) and bulk could not be completely avoided, as discussed in subsequent sections of this paper. It has been well documented that oxygen readily dissolves into nickel at elevated temperatures, with a threshold near 500 K [28,31,32]. This threshold for dissolution drops below 500 K for samples with large mosaic spreads [31] – a point which we shall revisit when we discuss singling kinetics in the next section. (These studies also imply that supposed "thermal desorption" runs which have been used by many researchers to clean various nickel surfaces most likely deposit much of the adsorbed oxygen into the bulk.) The detailed study by Holloway and Outlaw [32] is particularly relevant to our studies in that it demonstrates that sub-surface oxygen can modify the dissolution phase diagram, in particular increasing the concentration of oxygen which resides on the surface at a given temperature and oxygen exposure. Moreover, this study also showed that, at a given temperature, sub-surface oxygen can stabilize chemisorbed surface oxygen with respect to bulk dissolution, and even increase the temperature at which ordered overlayer structures can be observed. Such effects are cumulative for repeated oxygen exposures. These observations give us a scheme by which we can unify our structural and kinetic observations in the differing limits of trace and (repeated) large-scale oxygen exposure.

2.3. Scattering kinematics

In- and out-of-phase scattering kinematics, i.e., Bragg and anti-Bragg interference conditions, were intentionally used in this study to allow clear differentiation and detection of diffraction signatures from single and double stepped regions of the crystal. The helium beam energy and incident angle were chosen so that out-of-phase conditions for specular scattering ($\theta_i=\theta_f$) from the single-stepped surface are met:

$$kh(\cos\theta_i+\cos\theta_f)=2kh\cos\theta_i=(2n+1)\pi, \qquad (1)$$

where n is a integer. This judicious choice of scattering kinematics has the important effect of nulling the initial specular signal prior to the initiation of step-doubling. These same scattering conditions (which, to reiterate, are out-of phase for single steps) produce in-phase constructive interference for the double-stepped surface:

$$k(2h)(\cos\theta_i+\cos\theta_f)=4kh\cos\theta_i=2(2n+1)\pi=2m\pi, \qquad (2)$$

where n and m are integers, k is the momentum of the incident He beam ($k=6.48$ Å^{-1}, $\lambda=0.97$ Å), h is the single step height (2.032 Å), and θ_i (33.4°) is the incident angle of the He beam with respect to the terrace normal. This arrangement affords optimal sensitivity to the appearance and disappearance of double steps during the course of oxidation.

We now compare the relative merits of monitoring step-doubling/singling with the scattering plane aligned either parallel (plane S′ in Fig. 2b) or perpendicular (plane S in Fig. 2b) with respect to the step direction. At first thought it might seem preferable to choose across step scattering for all experiments. This configuration yields in-plane diffraction peaks due to the periodic grating of the steps, and therefore provides a clear signature for differing reciprocal lattices as shown, for example, in Fig. 1. However, in this geometry one must carefully deconvolve the (overlapping) peak intensities in order to quantify the concentration of single and double steps. When the scattering plane is aligned parallel to the steps, and in- and out-of-phase interference conditions with respect to adjacent terraces are used, this quantification problem is solved since no signal arises from single-stepped regions of the crystal. Moreover, the dynamic range of the measurement is also increased, allowing one to clearly monitor the *very* early phases of interface reconstruction. Fig. 3 shows a comparison of the diffraction intensities for single- and double-stepped surfaces using interference conditions which are constructive for the double-stepped interface but destructive for single-stepped terraces. The specular diffraction intensity from the single-stepped surface is due to residual imperfections following sample preparation. Typical initial conditions, as characterized by the residual signal shown in Fig. 3, were used in our kinetics measurements. The data of Fig. 3 emphasize the sensitivity of the method. In kinetic runs the small initial intensity was subtracted as a constant background for data analysis. The relative double-step density can be determined from the intensity of the lone specular diffraction peak. Further discussion of Bragg/anti-Bragg interferences for this surface can be found in Refs. [23,24]. Fig. 4a shows the specular diffraction peak growing in as a function of time with 0.0096 ML oxygen dosed at time = 0. From Fig. 4b, where the peak heights are normalized to 1, it is apparent that the peak widths are constant. Thus it is only necessary to monitor the height of the specular diffraction peak during kinetic measurements since the shape is constant.

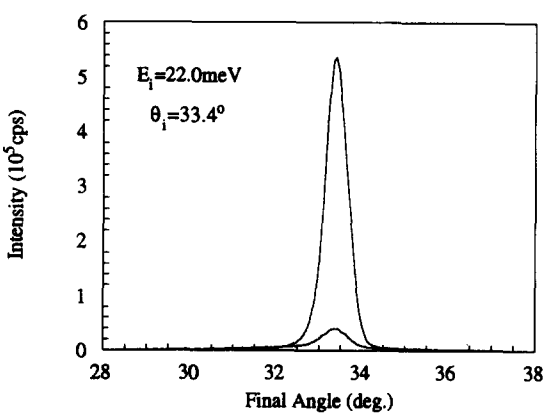

Fig. 3. Comparison of diffraction intensities between the clean single-stepped surface (out-of-phase, low signal) and substantially double-stepped surface (in-phase, high signal) for scattering along the step direction.

3. Results

3.1. Kinetics of step-doubling

We now present the isothermal and isosteric kinetic data for step-doubling induced by low coverages of adsorbed oxygen. Fig. 5a shows the raw specular diffraction intensity data, taken using out-of-phase interference conditions with respect to adjacent single steps, as described in the previous section. These data, taken with $T_s=450$ K, are shown as a function of time for different oxygen coverages, which span the range from 0.0036 ML of adsorbed O to just under 2% of a monolayer. Fig. 5b shows the extracted rate constants, while Fig. 5c presents the oxygen coverage dependence of the initial doubling rate. (These initial rates were extracted by taking linear fits to the first 5 data points of each data set of Fig. 5a.) At this temperature, the doubling rate increases until the oxygen coverage reaches 0.012 ML, above which the doubling rate levels off. Note that these data were taken in one day, beginning with a sputter cleaning

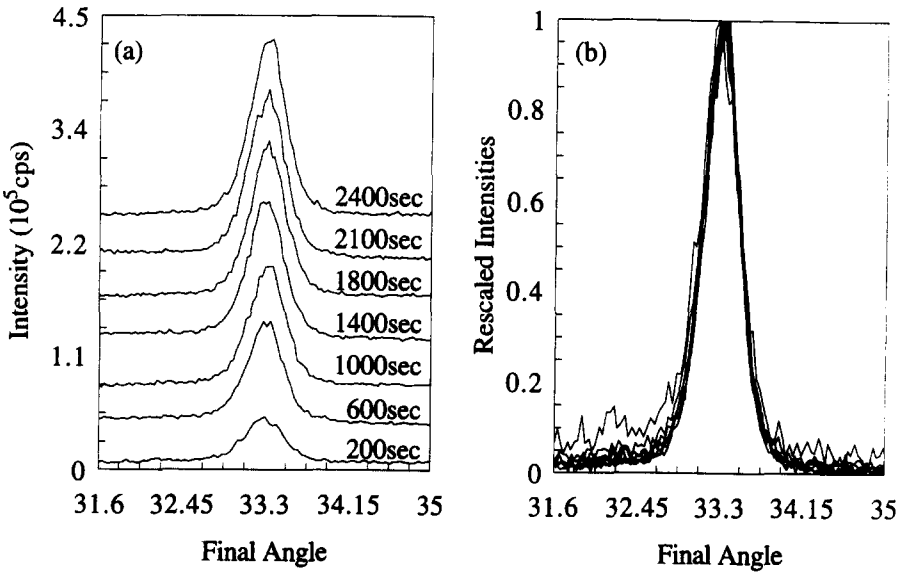

Fig. 4. Time evolution of the diffraction peak during step-doubling: (a) intensities at 200, 600, 1000, 1400, 1800, 2100 and 2400 s; (b) comparison of normalized lineshapes. $\theta_i = 33.4°$, $E_i = 22.0$ meV.

and anneal to remove oxygen from the surface and selvedge from the previous day. The runs were then taken in order of increasing oxygen exposure, separated by heating to 950 K to remove oxygen from the surface. The highest coverage runs may therefore have small amounts of dissolved oxygen in the near-surface region. Time constraints prohibited sputtering after every run.

The oxygen coverage dependence of the step-doubling kinetics provides insight into the microscopic mechanism: oxygen diffusion is not expected to be strongly coverage dependent or rate limiting at these dilute concentrations, while Ni atom diffusion across the terraces should not be significantly affected by oxygen adatoms primarily adsorbed at steps. (Supporting evidence that oxygen initially migrates to the step edge comes from our studies of step-edge-induced surface phonon modes on Ni(977) surface [23,24]. Here we observed that the step-edge-related phonon modes were preferentially quenched by small quantities of adsorbed oxygen.) This suggests that the initial rate-limiting step of this reconstruction is Ni atom mass transport. Such transport involves atoms leaving the step edge as well as step meandering (with meandering rates being influenced by both Ni diffusion along the step edge as well as detachment/reattachment mechanisms), rates which are altered by O adsorbed at the step. We infer from the above observations that the step-doubling transition is driven by the added thermodynamic stability for oxygen adsorbed at two-atom high step edges as compared to single-atom high structures in the limit of low oxygen coverages.

We now assess the kinetic order for the step-doubling transition. This entails two stages: we must link the observed scattering intensity to the density of double steps, and then ascertain whether first- or second-order kinetics provide a better description of the data. For first-order kinetics,

$$\frac{\mathrm{d}\{D\}}{\mathrm{d}t} = k_\mathrm{d}\{S\} = k_\mathrm{d}(1-\{D\}), \tag{3}$$

$$\{D\} = D_0(1-\exp(-k_\mathrm{d}t)), \tag{4}$$

where $\{D\}$ and $\{S\}$ are double- and single-step concentrations, and k_d is the rate constant for doubling. Hence the double step diffraction intensity is

$$I = I_0(1-\exp(-k_\mathrm{d}t))^n, \tag{5}$$

where n depends upon the coherence of the He

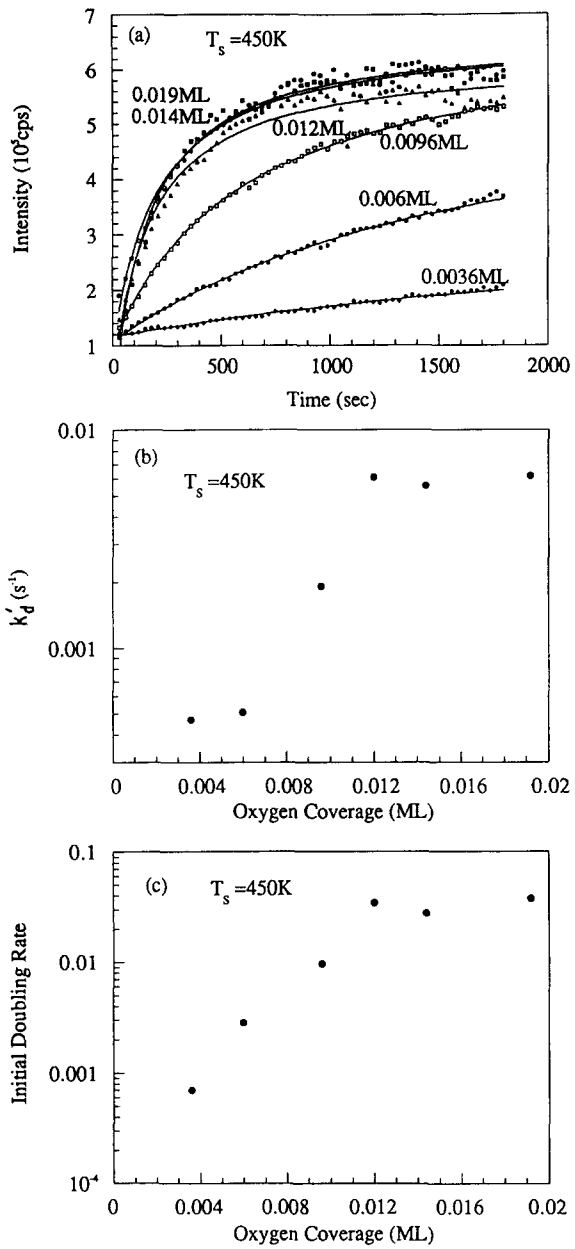

Fig. 5. Step-doubling as a function of oxygen coverage at a crystal temperature of 450 K: (a) raw data with fits to second-order kinetics; (b) rate constant obtained from fits; (c) initial doubling rate. Both rates levels off at about 0.012 ML of oxygen. $\theta_i = 33.4°$, $E_i = 22.0$ meV.

scattering, which may be morphology dependent. If the double-step population consists of large domains, then the He is scattered coherently and the intensity I is proportional to $\{D\}^2$, and $n=2$. If the double-step population consists of small domains, then the scattering will be incoherent and I will be proportional to $\{D\}$, and hence $n=1$. Intermediate values of n are obviously possible.

A similar discussion, now for second-order kinetics, gives the kinetic expression

$$\frac{d\{D\}}{dt} = k'_d \mathrm{Ma}S\}^2 = k'_d(1-\{D\})^2, \tag{6}$$

$$\{D\} = D_0\left(1 - \frac{1}{k'_d t + 1}\right), \tag{7}$$

where k'_d is the second-order rate constant for doubling. The time-dependent double step diffraction intensity is given in this scenario by

$$I = I_0\left(1 - \frac{1}{k'_d t + 1}\right)^n \tag{8}$$

Fig. 6 shows the results of a typical step-doubling experiment, where the double-step diffraction intensity is plotted as a function of time. There are four possible cases for the time dependence of the double-step diffraction intensity: first-order kinetics with incoherent He scattering, $I = I_0(1-\exp(-k_d t))$, as fitted to the data in Fig. 6a; first-order kinetics with coherent He scattering, $I = I_0(1-\exp(-k_d t))^2$, as fitted to the data in Fig. 6b; second-order kinetics with incoherent He scattering, $I = I_0\left(1 - \frac{1}{k'_d t + 1}\right)$, as fitted to the data in Fig. 6c; and second-order kinetics with coherent He scattering, $I = I_0\left(1 - \frac{1}{k'_d t + 1}\right)^2$, as fitted to the data in Fig. 6d. Second-order kinetics clearly give better fits than first-order kinetics. Distinguishing between coherent and incoherent He scattering is more subtle, but the incoherent model is better when examining the overall data set. Intermediate values of n were not examined in this study. (Activation energies derived from Arrhenius analysis are insensitive to the value of n; this is not the case for pre-exponential factors.)

As seen in Fig. 5, the rate for step-doubling decreases as the oxygen coverage decreases. We

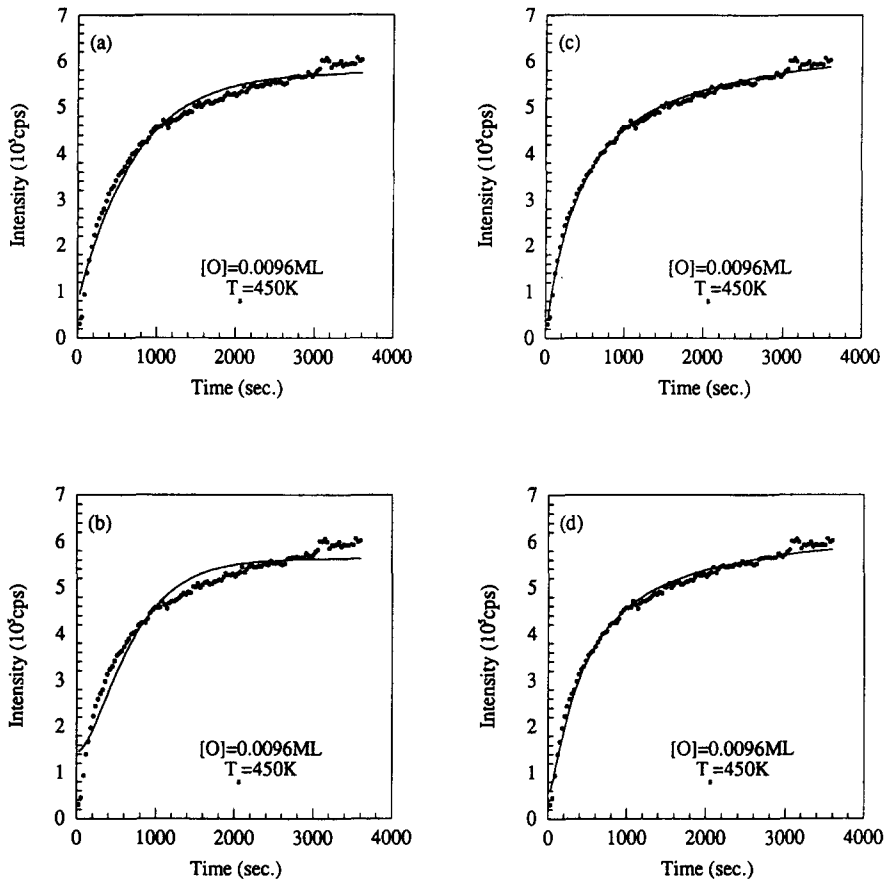

Fig. 6. Fitting trials for typical step-doubling data: (a) fit to $I_0(1-\exp(-Kt))$; (b) fit to $I_0(1-\exp(-Kt))^2$; (c) fit to $I_0(1-1/(1+Kt))$; (d) fit to $I_0(1-1/(1+Kt))^2$. $\theta_i=33.4°$, $E_i=22.0$ meV.

can use this to our advantage to better determine whether helium atoms are scattered incoherently or coherently from double steps by monitoring step-doubling in the limit of very low oxygen coverage (<0.004 ML) where kt is much less than unity. The double-step diffraction intensity can in this limit be expanded as a power series in kt, and the leading term will be either kt or $(kt)^2$. Fig. 7a plots double-step diffraction intensities as a function of time for different crystal temperatures with 0.0024 ML oxygen, along with linear fits to the experimental data. The data is clearly linear, indicating that the helium is scattered incoherently. This suggests that the double-step population exists as small domains.

Given that the kinetics of step-doubling is second order with respect to single-step density and that He atoms are scattered incoherently from the double-step population, let us now revisit the data of Fig. 5. The solid lines in Fig. 5a are the model fits using this analysis, while Fig. 5b shows the derived rate constants. The second-order model provides a quantitative description of the data. Moreover, the rate constant data set behaves qualitatively the same as the initial doubling rate, increasing steadily until a coverage of about 1% is reached. Fig. 8a shows the double-step diffraction intensities as a function of time for different crystal temperatures with 0.0096 ML oxygen, together with the model fits. The global agreement of the second-order kinetic model to these data is clear.

Arrhenius analysis was then used to extract information on the energetics of the step doubling.

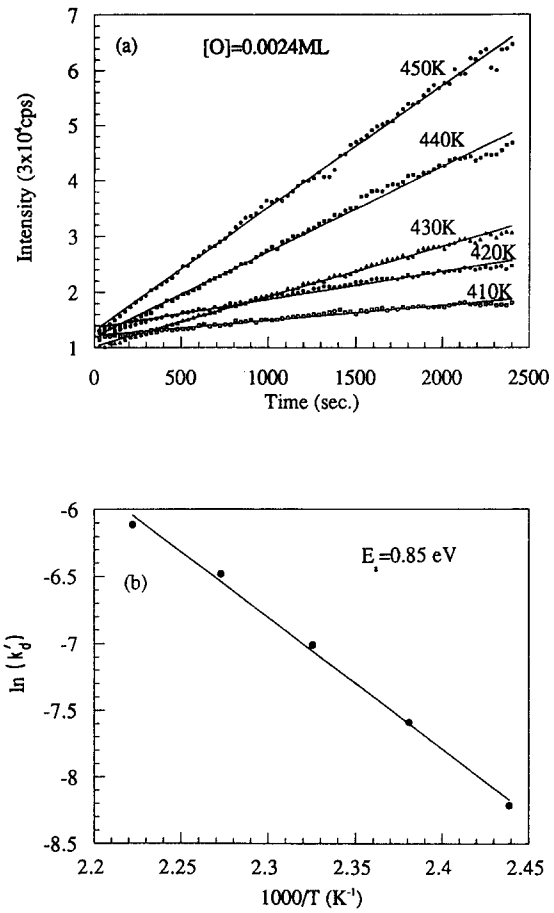

Fig. 7. Step-doubling: (a) linear fits to the double-step diffraction intensities as a function of time at different crystal temperatures with 0.0024 ML oxygen; (b) Arrhenius analysis of the process (see elaboration in text); $E_a = 0.85 \pm 0.04$ eV, $A_0 = 10^{6.9 \pm 0.4}$ s^{-1}. $\theta_i = 33.4°$, $E_i = 22.0$ meV.

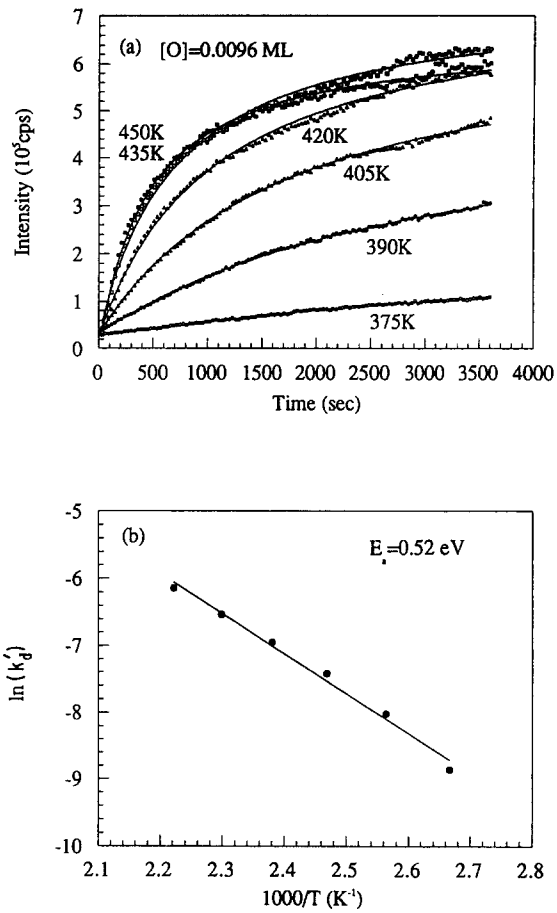

Fig. 8. Step-doubling: (a) fits of second-order kinetics to the double-step diffraction intensities as a function of time at different crystal temperatures with 0.0096 ML oxygen; (b) Arrhenius analysis of the process (see elaboration in text); $E_a = 0.52 \pm 0.03$ eV, $A_0 = 10^{3.1 \pm 0.3}$ s^{-1}. $\theta_i = 33.4°$, $E_i = 22.0$ meV.

We used the standard formula

$$K = A_0 \exp(-E_a/k_B T), \tag{9}$$

where E_a is the activation energy and A_0 is the pre-exponential factor. Figs. 7b and 8b show the results for two oxygen coverages: $E_a = 0.85 \pm 0.04$ eV, $A_0 = 10^{6.9 \pm 0.4}$ s^{-1} for [O] = 0.0024 ML, and $E_a = 0.52 \pm 0.03$ eV, $A_0 = 10^{3.1 \pm 0.3}$ s^{-1} for [O] = 0.0096 ML. The variance in both the activation energies and pre-exponential factors between these two data sets provides cautionary notes in two regards: first, that Arrhenius analysis should be applied with caution to small data sets over narrow temperature ranges, especially when some curvature may be present in the plots and, second, that slight differences in the immediate history of the sample with respect to oxygen dosing may influence the observed behavior (see the section 2 for elaboration). Data sets taken on individual days exhibit the most reliable trends, suggesting that the second issue, sample history and oxygen dissolution into the selvedge, is crucial. Nevertheless, to summarize the data without bias, we report that activation energies from 0.4 to 0.9 eV were observed. The lowest coverage data (which had the lowest integrated oxygen exposure) gave the high-

est value, $E_a = 0.85$ eV. Embedded atom method electronic structure calculations which examined the energetics for diffusion along and away from step edges predict adatom migration energies on stepped Ni(111) which fall in this range [33]. For comparison, we note that on Rh(332) Hoogers and King [11] found that $E_a = 1.1 \pm 0.1$ eV, $A_0 = 10^{11.0 \pm 0.9}$ s^{-1} for [O] = 0.1 ML.

3.2. Kinetics of step-singling

In this section we examine the kinetics for step singling of the double-stepped surface. Step singling in the limit of low oxygen coverages can be initiated by raising the surface temperature above 470 K. This process is reversible as shown in Fig. 9. Step-singling can also be initiated on a metastable (oxygen free) doubled surface by a similar increase in surface temperature to $T_s \geq 470$ K. As expected, the clean interface does not re-double upon the subsequent lowering of T_s.

Let us begin with the step-singling kinetic analysis by determining, for low coverages of initially adsorbed oxygen, the kinetic order as was done previously for the step-doubling transformation. We concluded in the previous section that He atoms are scattered incoherently from the double-step population, i.e., $n = 1$ in Eq. (8). For the case of first-order singling kinetics we have:

$$\frac{d\{S\}}{dt} = \frac{d(1-\{D\})}{dt} = k_s\{D\}, \tag{10}$$

$$\{D\} = D_0 \exp(-k_s t) \tag{11}$$

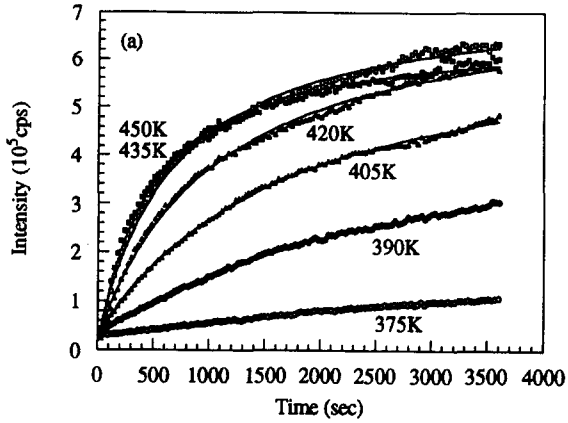

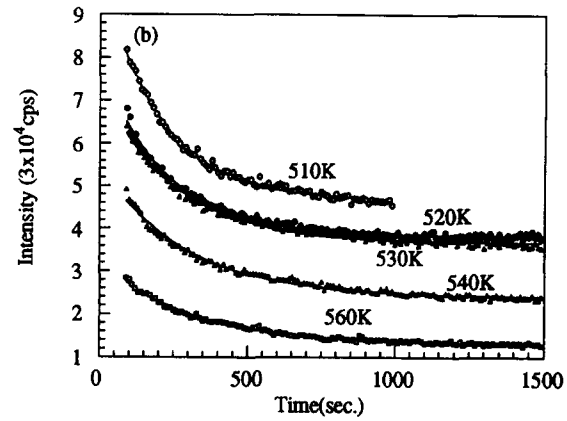

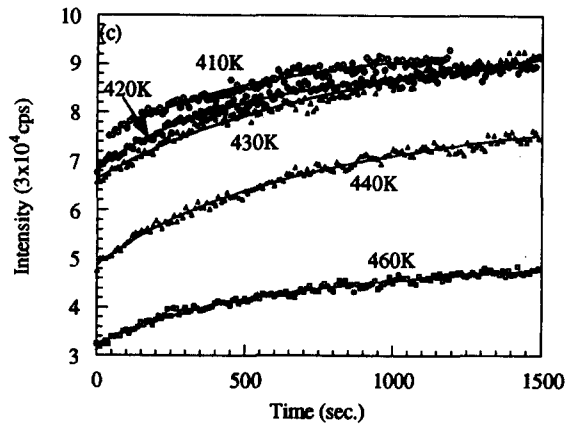

Fig. 9. Step-doubling/singling as a reversible structural transition at an oxygen coverage of 0.0096 ML. (a) Step-doubling at lower temperatures. (b) Step-singling at elevated temperatures following temperature jumps from 450 K. The early stages of step-singling were not recorded due to the finite time required for the crystal to reach and stabilize at the measurement temperature. (c) Step re-doubling after lowering the temperature below 470 K. The 410 K data come from a temperature jump of −100 degrees from the 510 K data of (b); similar −100 degree jumps connect the other data sets in panels (b) and (c). The early stages of step-doubling were not recorded in (c) due to the finite time required for the crystal to reach and stabilize at the measurement temperature.

with the double-step diffraction intensity given by

$$I = I_0 \exp(-k_s t). \tag{12}$$

If the kinetics are second order, the singling kinetics should behave as:

$$\frac{d\{S\}}{dt} = \frac{d(1-\{D\})}{dt} = k_s'\{D\}^2, \tag{13}$$

$$\{D\} = D_0\left(\frac{1}{k_s' t + 1}\right), \tag{14}$$

with the double-step diffraction intensity given by

$$I = I_0\left(\frac{1}{k_s' t + 1}\right). \tag{15}$$

The fits of these two models to the data are shown in Fig. 10 with unambiguous results: the data are best fit by first-order kinetics.

Fig. 11a shows the decrease in double-step diffraction intensity, as well as the corresponding first-order kinetic fits, for 0.0096 ML of adsorbed oxygen at a variety of surface temperatures above 470 K. These data were generated using the following procedure: the clean, single-stepped, 450 K surface was first dosed with oxygen. We then waited for about 40 min to let the surface double, and then abruptly raised the crystal temperature to initiate reversion to single steps. First-order modelling (the solid lines in the figure) provides global agreement with the data. Arrhenius analysis, based on four narrowly spaced temperatures in Fig. 11b, gives: $E_a = 1.7 \pm 0.1$ eV, $A_0 = 10^{14.8 \pm 1.0}$ s^{-1} for [O] = 0.0096 ML.

A metastable double-stepped but oxygen-free surface can be generated by exposing the system to hydrogen at moderate temperatures, similar to the procedures used by Comsa et al. in their study of Pt(997) [10]. After dosing the clean single-stepped surface with 0.006 ML oxygen at 450 K, we waited 40 min for the steps to double. Then, we exposed the surface to 3×10^{-7} Torr of hydrogen for 20 min, which removed the oxygen. Finally, the crystal temperature was raised above 470 K to observe step-singling. The decay of the double-step diffraction intensity as a function of time is shown in Fig. 12. Again, the data are best described using first-order kinetics. Arrhenius

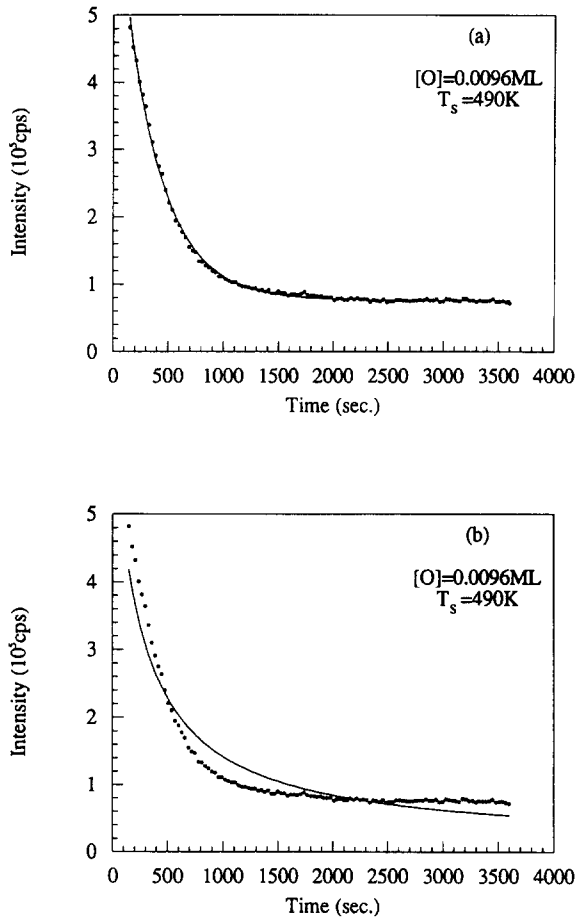

Fig. 10. Fitting trials for typical step-singling data: (a) fit to $I_0(1-\exp(-k_s t))$; (b) fit to $I_0(1-1/(1+k_s' t))$. $\theta_i = 33.4°$, $E_i = 22.0$ meV.

analysis (with some curvature in the plot; Fig. 12b), yields $E_a = 1.95 \pm 0.15$ eV and $A_0 = 10^{17.6 \pm 1.5}$ s^{-1}. On Pt(997), Comsa et al. [10] found $E_a = 1.8$ eV and $A_0 = 6 \times 10^{11}$ s^{-1}.

Our initial thoughts on the nearly identical singling kinetics for the oxygen-free and oxygen-containing surfaces centered on the entropy contribution to the free energy of the system being dominant above 470 K. However, further exploration of the literature turned up several articles which demonstrate that oxygen dissolves into Ni around 500 K [28,31,32,34]. Moreover, Kortan and Park noted that samples with large mosaic spreads exhibited dissolution temperatures below this point [31] probably due to the higher density

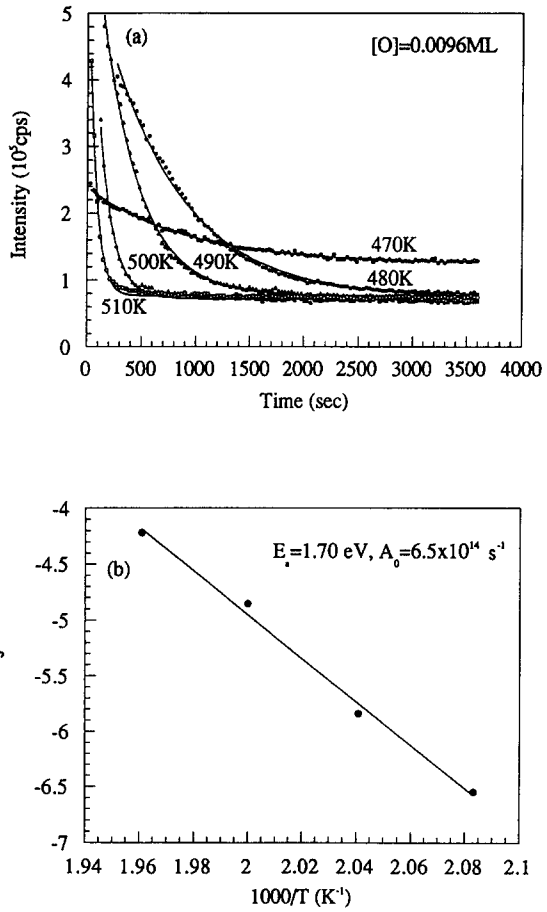

Fig. 11. Step-singling with oxygen. (a) First order kinetic fits to the decay of double-step diffraction intensities as a function of time at different crystal temperatures with 0.0096 ML oxygen. (b) Arrhenius analysis of the data. $\theta_i = 33.4°$, $E_i =$ 22.0 meV.

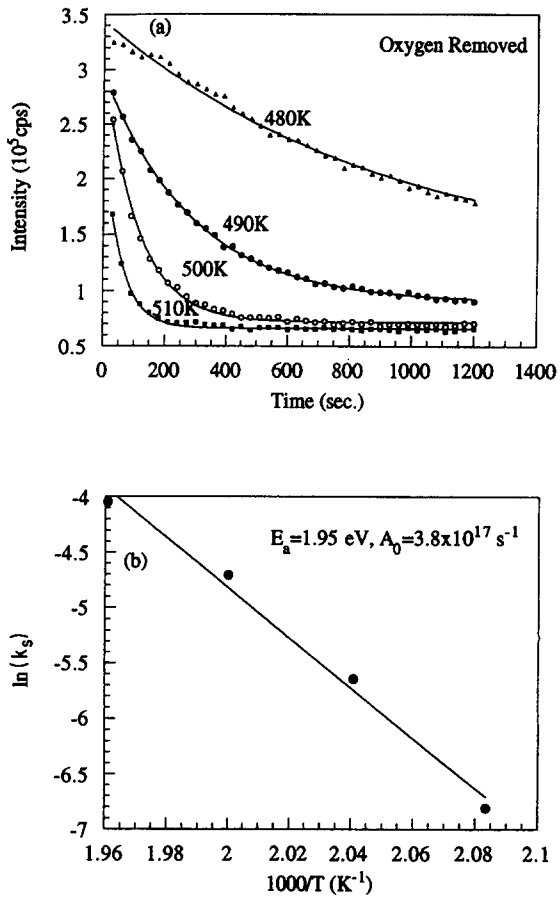

Fig. 12. Step-singling without oxygen. (a) First-order kinetic fits to the decay of double-step diffraction intensities as a function of time at different crystal temperatures following hydrogen reduction of 0.006 ML oxygen. (b) Arrhenius analysis of the data. $\theta_i = 33.4°$, $E_i = 22.0$ meV.

of grain boundaries on such surfaces. These observations lead us to speculate that the small quantities of adsorbed oxygen in this study may in fact dissolve into the bulk or selvedge region near 470 K, and lead to the identical kinetic behavior for the apparently oxygen-containing and oxygen-free samples. Furthermore, it has also been reported that the stability range for chemisorbed overlayers can depend on the amount of oxygen dissolved near the surface [32], with sub-surface oxygen tending to enhance the amount of oxygen on the surface at a given temperature and exposure. Clearly the chemical potential of the selvedge region can be modified by the presence of oxygen, thermodynamically influencing the partitioning between adsorbed and absorbed species. This can account for the onset of doubling at temperatures above 470 K when higher exposures of oxygen are used (Fig. 1), a point more thoroughly discussed in our earlier paper on this subject [14].

The initial kinetic competition between step-doubling and step-singling is another interesting regime which can be seen at low oxygen coverages in a narrow temperature range just at or above 470 K. Fig. 13 shows such competitive behavior for two oxygen coverages. As shown in the upper panel,

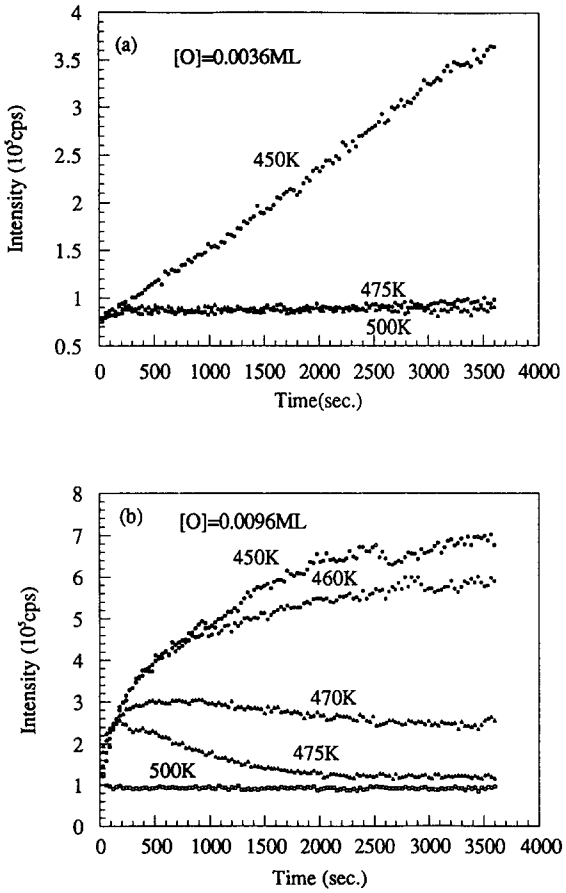

Fig. 13. Step doubling/singling kinetics at low oxygen coverages and temperatures in the vicinity of 470 K. Competitive kinetics can be seen between doubling and singling for 470 and 475 K in the lower panel.

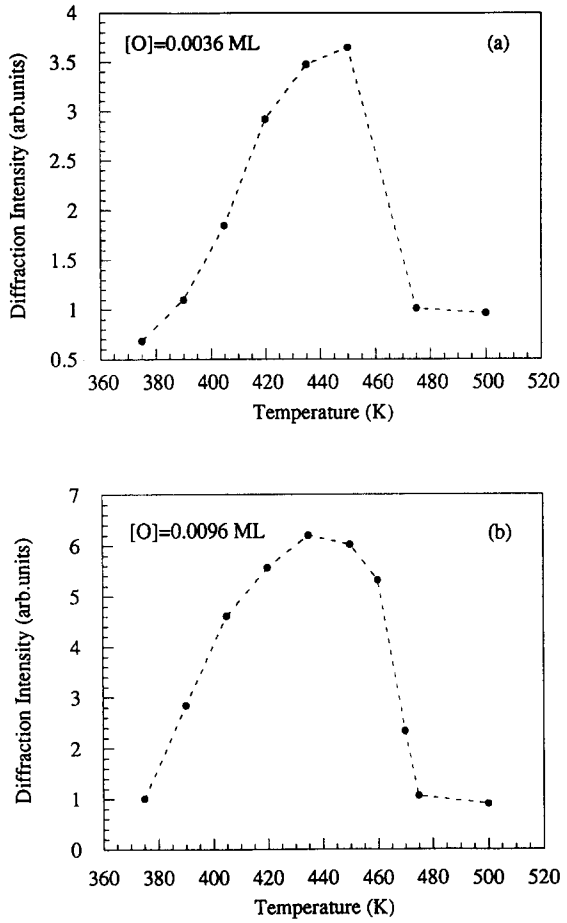

Fig. 14. Diffraction intensities (linearly proportional to the double-step population) as a function of crystal temperature 40 min after oxygen dosing. (a) [O] = 0.0036 ML; (b) [O] = 0.0096 ML.

at an oxygen coverage of 0.0036 ML, the system remains singled for $T_s \geq 470$ K. In contrast to this, the higher coverage data shown in the lower panel of Fig. 13 have a visible kinetic window where the surface initially starts to double, but then reverts to a singled structure for 470 and 475 K; by 500 K this kinetic window has closed and the surface does not begin to double. This behavior suggests a delicate balance between several kinetic and thermodynamic concerns, such as the relative rates of oxygen diffusion to step edges versus dissolution into the bulk. Such kinetic regimes will be most fruitfully explored when detailed atomic level spatial maps of the initial structure are available. We therefore defer further analysis until STM images of our sample are in hand.

Finally, in Fig. 14 we present stability regimes for the conditions used in Fig. 13. Here, we see that at low temperatures ($T_s \leq 375$ K) doubling does not initiate – presumably due to the lack of Ni diffusional mobility at such low temperatures. At the other extreme, we see that the region of double-step stability (for very low coverages of oxygen) ends at $T_s \approx 470$ K, presumably due to step-entropy effects and temperature-dependent oxygen partitioning between the step edges, terraces, and bulk.

4. Discussion and conclusions

In this paper we have examined the kinetics for the oxygen-driven step-doubling and -singling of Ni(977) in the limit of very low coverages of oxygen. These reconstructions precede the onset of bulk oxidation and occur over a temperature regime which is bounded at low temperatures by the limited thermally activated diffusion of Ni. At intermediate temperatures the situation is a bit more complex, depending on the extent of oxygen adsorption and the temperature/dosing history of the substrate during a given run. At high temperatures, $T_s \geq 470$ K, no doubling is observed, probably due to a combination of bulk dissolution of surface-adsorbed oxygen and entropy contributions which favor step-singling. At the low coverages we focussed on in this paper, we have seen a reversible phase transition in the vicinity of 470 K at which the doubled structure reverts to a single-stepped one. This is presumably due to $T\Delta S$ contributions to the surface free energy which favor single steps. (Changes in the partitioning of oxygen between terraces and steps at elevated temperatures may also play a role in inducing such transformations.)

Our observations imply that the thermodynamic driving force for the doubling is supplied when O adsorbs at doubled (100) step-edges. This is reasonable, especially given studies which show that oxygen initially adsorbs in four-fold hollow sites on the (100) surface [28]. At higher oxygen coverages the presence of additional oxygen on the terraces destabilizes this reconstruction [14]. This behavior is similar to work on Rh(332) (a surface with (111) oriented terraces and step edges), where continued oxygen dosing again leads to a re-singling of the surface [11]. The singling data is also interesting in another way: the activation energies we observed for our surface is about 1.7 eV with 1% initial oxygen dosing and 1.9 eV for the oxygen-free surface, values which are identical within our experimental precision. These results suggest a common intermediate condition which connects these systems. Bulk dissolution of trace surface adsorbed oxygen is one possibility, leaving the systems in identical states above 470 K. This point is extensively covered in the previous section.

The kinetics were probed using in- and out-of-phase (i.e., Bragg and anti-Bragg) helium scattering interferences with respect to double- and single-step heights, respectively. This methodology, using scattering kinematics aligned along the step direction, afforded high sensitivity to the onset of step doubling. Using this, we first explored the kinetics of step-doubling for Ni(977) induced by low coverages of oxygen as a function of oxygen coverage and surface temperature. The kinetics were shown to be second order in the single-step density. This conclusion was reached after considering the possibility of first- or second-order kinetics in this parameter. Moreover, modelling of an extensive data set also revealed that the observed scattering was incoherent, indicating the presence of rather small domains during the initial stages of this transformation. Second-order kinetics with respect to single-step density agrees with the Hoogers and King [11] findings for step-doubling on Rh(332) induced by 0.1 ML oxygen. This is not surprising since both studies are in the low oxygen coverage regime. We note that first-order step-doubling kinetics were previously reported for Pt(997) by Comsa et al. [10] using higher oxygen coverages. This suggests that the nature of such structural transformations are not universal, but rather are sensitive to the amount of oxygen (density of pinning centers) present as well as the specific properties of a given vicinal surface. The system's history, i.e., the detailed time and temperature-dependent dosing procedures used, may also influence its kinetic evolution. The activation energies for Ni atoms leaving the step edge, step meandering via diffusion along the step edge, and Ni atoms stepping down/jumping over the step may all be influenced by the presence of oxygen.

The observation of second-order kinetics with respect to the single-step density deserves comment. Hoogers and King [11] suggested a series of coupled differential equations which considered the rate of atom migration away from single and double steps, as well as the rate of migration along a step or across a terrace. For doubling, they derived an analytic rate expression by assuming that the reverse detachment of atoms from the doubled step was negligible, as well as a steady-state atom population in the mobile phase (on

terraces and for movement along the step edge). Their solution within these approximations is identical to our result, Eqs. (6–8), and thus indicates some common ground for these two studies. The activation energy found in Fig. 7 has $E_a = 0.85$ eV, or 82 kJ/mol. This is slightly lower than the 108 kJ/mol value for Rh(332), consistent with the lower enthalpy of evaporation [35] for Ni (429.7 kJ/mol) versus Rh (556.9 kJ/mol). (Hoogers and King note that 1/6 of this thermodynamic quantity is a useful measure of the energy required for breaking a single bond in a metal; the Rh/Ni ratios of these two parameters are interestingly 1.3 for both E_a and ΔH_f°.)

After preparing double-stepped surfaces using low coverages of oxygen, step-singling kinetics were examined by jumping to various temperatures with $T_s \geq 470$ K. These step-singling measurements were done with and without oxygen present. The oxygen-free measurements utilized a metastable interface which was prepared using hydrogen to burn off the adsorbed oxygen. The step-singling kinetics were found to be first order in the double step density with low oxygen coverages as well as with no oxygen present. This is reminiscent of the behavior observed for Pt(997) with the oxygen removed [10]. The second-order kinetics observed for step-singling of Rh(332) is for a higher oxygen coverage (0.6 ML). This again suggests that the amount of oxygen and detailed time-dependent history of the sample dosing can influence the kinetics of this extensive reconstruction.

The time is now clearly ripe for an STM experiment to examine the microscopic real-space and real-time dynamics of this, and other step-doubling/singling systems. The ability of STM to distinguish singles and doubles is clear, as has been shown, for example, in recent work on Ni(771) [8,9], Mo(100) [12], and Pt(997) [13]. Such measurements would nicely complement the kinetic database now in hand, and would hopefully reveal additional details of how step-adsorbed oxygen influences the rate at which Ni atoms detach from the step edge and migrate over the step region from one terrace to the next. Information on the location of adsorbed oxygen as a function of coverage might also be extracted from such measurements [36]. In situ atomic level microscopy could quantify how step-edge roughness (kinks) influence the reconstruction dynamics. Such imaging would also reveal how step meandering contributes to the doubling mechanism, i.e., whether one should view this as a "zippering" process in which one point of contact (pinning connection) between adjacent steps greatly accelerates step merging. Theoretical work along these lines using Monte Carlo simulations has recently been reported by Khare et al. [37]. These simulations examined some preliminary data from our laboratory, as well as kinetic data for Rh(332). The combination of experimental data of the type presented herein with Monte Carlo and molecular dynamics should, moreover, allow critical tests of electronic structure calculations which give values for adatom diffusion away from step edges, along step edges, and across terraces [33], as well as the importance of step meandering in the coalescence process [37,38].

To summarize, helium atom scattering has been used to study the kinetics for step-doubling on Ni(977) induced by very low coverages of oxygen (<2% of a monolayer) as a function of surface temperature and adsorbate coverage. Oxygen adsorbed at steps provides the thermodynamic driving force for this transformation. Step-singling kinetics have also been examined for low oxygen coverages, as well as the metastable oxygen-free but doubled surface. These measurements provide benchmark data for theoretical models which seek to understand both the energetics and kinetic paths by which such transformations occur. Moreover, they provide new details of the initial stages of oxidation which a defect containing metallic interface evolves through prior to the onset of deeper levels of oxidation. Such knowledge may ultimately enhance our ability to tailor interfacial properties in order to minimize or retard the onset of bulk oxidation.

Acknowledgements

We would like to thank Kevin Gibson and Jennifer Colonell for many helpful discussions. This work was supported by the Air Force Office of Scientific Research and, in part, the NSF Materials

Research Science and Engineering Center at the University of Chicago, NSF-DMR-9400379.

References

[1] G.A. Somorjai, Chemistry in Two Dimensions: Surfaces (Cornell Univ. Press, Ithaca, 1981).
[2] B. Lang, R.W. Joyner and G.A. Somorjai, Surf. Sci. 30 (1972) 454.
[3] D.W. Blakely and G.A. Somorjai, Surf. Sci. 65 (1977) 419.
[4] H.V. Thapliyal and J.M. Blakely, J. Vac. Sci. Technol. 15 (1978) 600–605.
[5] H.V. Thapliyal, PhD Thesis, Cornell University, 1978.
[6] J.P. Chang and J.M. Blakely, J. Vac. Sci. Tech. A 10 (1992) 2154.
[7] D.G. Castner and G.A. Somorjai, Surf. Sci. 83 (1979) 60.
[8] O. Haase, R. Koch, M. Borbonus and K.H. Rieder, Phys. Rev. Lett. 66 (1991) 1725.
[9] R. Koch, O. Haase, M. Borbonus and K.H. Rieder, Surf. Sci. 272 (1992) 17.
[10] G. Cosma, G. Mechtersheimer and B. Poelsema, Surf. Sci. 119 (1982) 159.
[11] G. Hoogers and D.A. King, Surf. Sci. 286 (1993) 306.
[12] J.C. Dunphy, C. Knight, P. Sautet, D.F. Ogletree, G.A. Somorjai and M.B. Salmeron, Surf. Sci. 280 (1992) 313.
[13] E. Hahn, H. Schief, V. Marsico, A. Frick and K. Kern, Phys. Rev. Lett. 72 (1994) 3378.
[14] D.D. Koleske, L. Niu, S.F. King and S.J. Sibener, to be published.
[15] O.L. Alerhand, A.N. Berker, J.D. Joannopoulos, D. Vanderbilt, R.J. Hamers and J.E. Demuth, Phys. Rev. Lett. 64 (1990) 2406.
[16] E. Pehlke and J. Tersoff, Phys. Rev. Lett. 67 (1991) 1290.
[17] T.M. Jung, R.J. Phaneuf and E.D. Williams, Surf. Sci. 254 (1991) 235.
[18] M.J. Stirniman, Wei Li and S.J. Sibener, J. Chem. Phys. 103 (1995) 451.
[19] Wei Li, M.J. Stirniman and S.J. Sibener, Surf. Sci. Lett. 329 (1995) L593.
[20] Wei Li, M.J. Stirniman and S.J. Sibener, J. Vac. Sci. Technol. A 13 (1995) 1574.
[21] W. Menezes, P. Knipp, G. Tisdale and S.J. Sibener, Phys. Rev. B 41 (1990) 5628.
[22] G. Tisdale and S.J. Sibener, Surf. Sci. 311 (1994) 360.
[23] L. Niu, D.J. Gaspar and S.J. Sibener, Science 268 (1995) 847.
[24] L. Niu, D.D. Koleske, D.J. Gaspar and S.J. Sibener, J. Chem. Phys. 102 (1995) 9077.
[25] B. Gans, S.F. King, P.A. Knipp, D.D. Koleske and S.J. Sibener, Surf. Sci. 264 (1992) 81.
[26] M.A. Van Hove and G.A. Somorjai, Surf. Sci. 92 (1980) 489.
[27] A. Winkler, K.D. Rendulic and K. Wendl, Appl. Surf. Sci. 14 (1983) 209.
[28] C.R. Brundle and J.Q. Broughton, in The Chemical Physics of Solid Surfaces and Heterogeneous Catalysis, eds. D.A. King and D.P. Woodruff (Elsevier, Amsterdam, 1990) Vol. 3A.
[29] D.F. Mitchell, P.B. Sewell and M. Cohen, Surf. Sci. 61 (1976) 355.
[30] T.S. Rahman, D.L. Mills, J.E. Black, J.M. Szeftel, S. Lehwald and H. Ibach, Phys. Rev. B 30 (1984) 589.
[31] A.R. Kortan and Robert L. Park, Phys. Rev. B 23 (1981) 6340.
[32] P.H. Holloway and R.A. Outlaw, Surf. Sci. 111 (1981) 300.
[33] Chun-Li Liu and James B. Adams, Surf. Sci. 265 (1992) 262.
[34] Paul H. Holloway, J. Vac. Sci. Technol. 18 (1981) 653.
[35] CRC Handbook of Chemistry and Physics, 75th ed. (CRC Press, Boca Raton, FL, 1994).
[36] M. Sokolowski, H. Pfnur and M. Lindroos, Surf. Sci. 278 (1992) 87.
[37] S.V. Khare, T.L. Einstein and N.C. Bartelt, Surf. Sci. 339 (1995) 353.
[38] K.D. Hammonds and R.M. Lynden-Bell, Surf. Sci. 278 (1992) 437.